Photoelectron Spectroscopic and Theoretical Studies of $M_mC_6F_5$ Anionic Complexes (M = Pb and Bi; $m = 1-4$)

Zhang Sun, Shutao Sun, Hongtao Liu, Qihe Zhu, and Zhen Gao*

Beijing National Laboratory for Molecular Sciences, State Key Laboratory of Molecular Reaction Dynamics, Center of Molecular Science, Institute of Chemistry, Chinese Academy of Sciences, Beijing 100080, People's Republic of China

Zichao Tang#

Beijing National Laboratory for Molecular Sciences, State Key Laboratory of Molecular Reaction Dynamics, Center of Molecular Science, Institute of Chemistry, Chinese Academy of Sciences, Beijing 100080, People's Republic of China, and State Key Laboratory of Molecular Reaction Dynamics, Dalian Institute of Chemical Physics, Chinese Academy of Sciences, Dalian 116023, People's Republic of China

Received: November 12, 2008; Revised Manuscript Received: May 25, 2009

The reactions between metal (Pb or Bi) clusters formed by laser ablation and hexafluorobenzene (C_6F_6) seeded in argon carrier gas were studied by a reflectron time-of-flight mass spectrometer combined with a photoelectron spectrometer. The adiabatic electron affinities of the dominant anionic products, $Pb_mC_6F_5^-$ and $Bi_mC_6F_5^-$ ($m = 1-4$) complexes, were obtained from the photoelectron spectra with 193 nm photons. It was found that the EAs of $Pb_mC_6F_5$ are higher than those of the pure Pb_m clusters and that the photoelectron spectra of $Bi_mC_6F_5^-$ show some similarities to those of Bi_{m+1}^-. Theoretical calculations were carried out to elucidate their geometric structures and bonding modes. The adiabatic detachment energy and simulated spectrum based on Koopmans' theorem for the optimized structures of each complex were in agreement with the photoelectron spectroscopy results. The most likely structures for each species were obtained. The analysis of the molecular orbital composition provides evidence that the C_6F_5 group contributes a single electron to bind with metal clusters through the M−C σ bond.

1. Introduction

The study of the adsorption of a molecule or fragment on a metal surface is an important subject in surface science.[1−3] The understanding of the structure and properties of adsorbates on metals can help to develop a microscopic level description of heterogeneous catalysis, organometallic reactions in the condensed phase, and electron transfer in biological systems.[4−10] Because the active site in the catalytic reaction is localized near the edge or defect of metal surface, the study of fragments adsorbed on small metal clusters can be a promising model for the understanding of catalysis and nanoassembly. It was reported recently that the steric effect strongly influences the adsorption of molecules onto metal surfaces. This report clarifies the dynamics in the entrance channels of the potential energy surfaces controlling the catalytic process.[11]

In recent years, many experimental[12−17] and theoretical[18−21] investigations of the interaction of metal clusters with benzene in the gas phase have been reported. Similarly, the interaction of metal with phenyl fragment was also studied. Xing et al.[22] reported the generation of $[M_m\text{phenyl}]^-$ (M=Mn−Cu) complexes. The phenyl−metal complexes $Ag_mC_6H_5^-$, $Au_mC_6H_5^-$ ($m = 1-3$),[23] and $Pb_mC_6H_5^-$ ($m = 1-5$)[24] were studied by photoelectron spectroscopy (PES) and density functional theory (DFT). Hexafluorobenzene is fully fluorinated, and the study of fluorine substitution on the benzene ring can help to understand the effect on bond strength of ionic π complexes. Fluorine substitution might strengthen metal anionic binding.[25,26] There are a few reports on the reactions of metals with C_6F_6.[25−27] The Kaya group[25] studied $(C_6F_6)_n^-$ and $Au(C_6F_6)^-$ complexes by photoelectron spectroscopy. Dunbar et al.[26] studied the reactions of Au^+ and Au^- with C_6F_6. However, little is known about the possibility of the attachment of metal anion to π face of hexafluorobenzene or to the fragment of hexafluorobenzene.

Lead is the heaviest element in group-IV, and bulk lead is metallic, in contrast to the semiconductors silicon and germanium. The structure of lead clusters is intriguing among the clusters of group-IV due to its large relativistic effects and especially spin−orbit coupling.[28,29] The studies of lead clusters have been reported by PES.[30−33] In industry, lead is involved in some important catalytic processes.[34,35] Several decades ago, Castleman and co-workers[36] reported the reaction of benzene with lead ions and showed that Pb^+−benzene displayed an unusually strong interaction.[37] Recently, we studied the reactions of lead anionic clusters with benzene[24,38] and pyridine[39] and found several series of products, such as $[Pb_m\text{-Phenyl}]^-$ ($m = 1-5$) and $[Pb_m\text{-Pyridyl}]^-$ ($m = 1-4$), which have not been detected before. However, the interactions between lead anionic clusters and C_6F_6 have not been reported.

Bismuth, the heaviest group V element, has attracted particular interest since bismuth nanowires and bismuth nanotubes (BiNTs) were fabricated.[40−42] Bi nanostructures as functional devices may motivate new applications, such as those in quantum transport, nanostructured lighting, and nanosensors.[43,44] The experimental study reported the fragmentation behavior of cationic Bi_n^+ ($n = 1-14$) clusters.[45,46] Rovner et al.[47] determined the dissociation energies of very small bismuth clusters Bi_n (n

* To whom correspondence should be addressed. E-mail: gaoz@iccas.ac.cn.
# zctang@dicp.ac.cn.

10.1021/jp8099626 CCC: $40.75
Published on Web 06/18/2009

= 2−4) by mass spectrometry. Polak et al.[48] recorded the photoelectron spectra of Bi_n^- (n = 2−4) clusters and investigated their electronic structures in detail, including the adiabatic electron affinity. Gausa et al.[49] measured the PE spectra of Bi_n^- (n = 2−9) at 4.03 eV photon energy and those of Bi_n^- (n = 2−21) at 5.0 eV photon energy. Gao et al.[50] studied the geometric and electronic structures of Bi_n and Bi_n^- clusters (n = 2−13) by first-principles simulations. However, the interactions between bismuth anionic clusters and aromatic molecules have not been reported.

In this paper, we report a new study of the anionic complexes $M_mC_6F_5^-$ (M= Pb and Bi; m = 1−4) by mass spectrometry and PES. The anionic complexes $M_mC_6F_5^-$ were produced in the reactions between C_6F_6 and metal clusters generated by laser ablation. By a combination of experimental and theoretical studies, the bonding, geometric and electronic structure, and orbital composition of the $M_mC_6F_5^-$ (M= Pb and Bi; m = 1−4) were obtained. The results might provide some fundamental information for future studies of physics and chemistry of heavy metal cluster complexes.

2. Experimental Methods

The apparatus used in the experiments mainly consists of a homemade reflectron time-of-flight mass spectrometer (RTOF-MS) and a magnetic-bottle photoelectron spectrometer. The details of the apparatus have been published elsewhere,[51,52] and only an outline is given below.

The metal disk target (Pb or Bi purity >99.99%) in the source chamber of reflectron time-of-flight mass spectrometry (RTOF-MS) was ablated by a pulsed laser beam (1064 or 532 nm Nd: YAG laser, 5 Hz, ~10 mJ/pulse), and the target was rotated during the experiments. The laser-induced plasma was carried by a molecular beam generated from a pulsed valve at a backing pressure of about 400 kPa of argon (purity 99.99%), in which C_6F_6 was seeded. The volume ratio of C_6F_6 in the mixed gas is about 0.1%. The anionic products generated by the reaction of the metal plasma with C_6F_6 were entrained by the carrier gas and underwent low pressure (10^{-2} Pa) in the source chamber. After passing a skimmer, all products entered into the acceleration area in the spectroscopic chamber of RTOF-MS (10^{-4} Pa). The anionic products were accelerated in the direction perpendicular to the molecular beam and were reflected toward double microchannel plates (MCP). The resolution ($M/\Delta M$) of RTOF-MS is better than 2000, so the anionic species can be easily assigned by the mass spectrum.

The anionic products were mass selected by the timing probe and were photodetached by an excimer laser (XeCl 308 nm or ArF 193 nm). The photoelectrons detached were measured by the magnetic-bottle photoelectron spectrometer. The PE spectra were calibrated with the known spectra of Ag^- and Au^-. The energy resolution of the photoelectron spectrometer is about 70 meV for electrons with 1 eV kinetic energy. However, the resolution is getting worse as the kinetic energy of the photoelectrons increases.

3. Computational Methods

Full geometric optimizations for all the studied cluster structures were performed with relativistic density functional calculations at the level of generalized gradient approach, using a Perdew−Wang exchange-correlation functional.[53] The zero-order regular approximation Hamiltonian was used to account for the scalar (mass velocity, Darwin, and spin−orbit) relativistic effects.[54] The standard Slater-type orbital basis sets of the triple-ζ plus two polarization functions (TZ2P) were used for the orbitals of Pb, Bi, C, and F atoms. And the frozen core ($1s^2-4f^{14}$) approximation was used for Pb and Bi. All the calculations were accomplished with the Amsterdam density functional (ADF 2005)[55] programs. It has been shown previously that these theoretical methods were suitable for the study of metal clusters.[56−58]

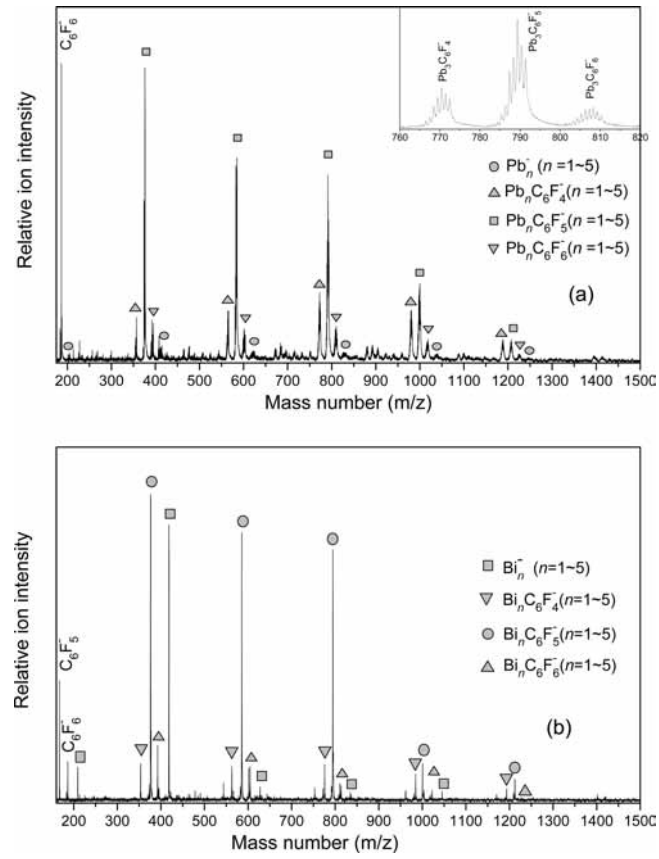

Figure 1. Typical mass spectra of the anionic products from the reactions between metal (M = (a) Pb and (b) Bi) by laser ablation and hexafluorobenzene seeded in argon carrier gas (0.1% hexafluorobenzene in 400 kPa mixed gas). The inset in Figure 1a shows the enlarged part of the spectrum.

4. Results and Discussion

4.1. Mass Spectrum. Parts a and b of Figure 1 show the typical mass spectra of the anionic products obtained from the reactions of lead or bismuth clusters generated by laser ablation with C_6F_6 seeded in argon carrier gas. All the mass spectra were calibrated carefully according to the mass numbers of pure metal clusters. The enlarged part in Figure 1a shows the isotope peaks of $Pb_3C_6F_5^-$, which can be resolved clearly.

As shown in Figure 1, there are three different series of the species: $M_mC_6F_4^-$, $M_mC_6F_5^-$ and $M_mC_6F_6^-$ (M = Pb and Bi; m = 1−5), and the $M_mC_6F_5^-$ complexes are the dominant products, suggesting their enhanced stabilities. The formation mechanism of the above species probably involves the selective cleavage of C−F bond in C_6F_6, similar to the formation of the Pb_m-phenyl complexes, discussed in our former publication.[38]

4.2. PE Spectra. The PE spectra of Pb_m^- and Bi_m^- (m = 2−4) at 308 nm (4.03 eV) photons are shown in Figure 2. The position, indicated with the arrow, is considered as the EA of every corresponding species. The adiabatic EA values are listed in Table 1. The measured EA values of Pb_m^- and Bi_m^- (m = 2−4), and their spectrum features are consistent with previous results.[31−33,48,49]

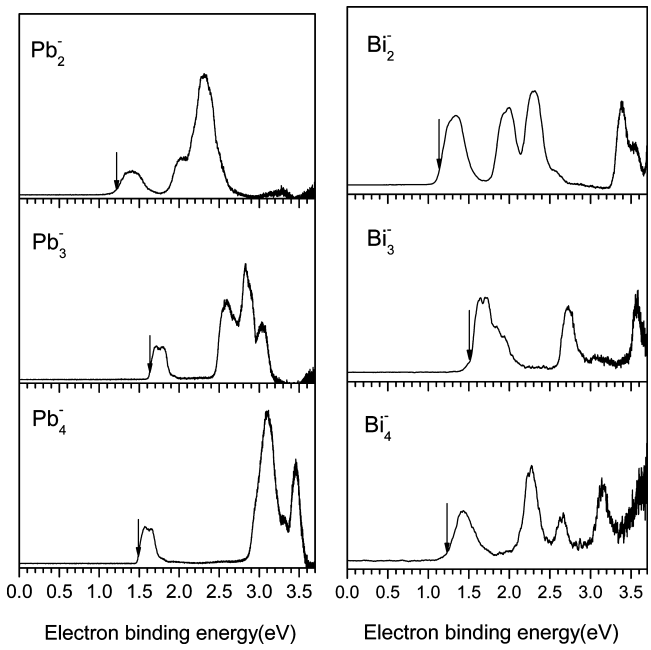

Figure 2. Photoelectron spectra of Pb_m^- and Bi_m^- ($m = 2-4$) at 308-nm (4.03 eV) photons.

TABLE 1: Observed EA for Pb_m and Bi_m ($m = 2-4$) (Uncertainty within ±0.1 eV)

	EA (eV)	
m	Pb_m	Bi_m
2	1.21 (1.37[a], 1.45[b])	1.22 (1.22[d], 1.271[e])
3	1.63 (1.70[b])	1.51 (1.48[d], 1.60[e])
4	1.50 (1.55[b], 1.37[c])	1.23 (1.15[d], 1.05[e])

[a] Reference 32, according to the Franck−Condon simulation. [b] References 31 and 48, the maximum of the first feature. [c] References 33 and 49, threshold of electron detachment. [d] References 33 and 49, threshold of electron detachment. [e] References 31 and 48, the maximum of the first feature.

The PE spectra of $Pb_mC_6F_5^-$ and $Bi_mC_6F_5^-$ ($m = 1-4$) at 193 nm (6.42 eV) photons are shown in Figure 3. It can be seen that the EA value of $Pb_mC_6F_5^-$ increases with the increase of m, Pb atom number. This tendency can be explained by the effect of the metal clusters on the outer valence electron. These complexes are all closed-shell electron system. So the more metal atoms the complex contains, the stronger effect of the metal cluster the outer electron in the metal cluster will feel. Therefore, the EA increases. However, the EAs of $Bi_mC_6F_5^-$ show the odd−even alternation, in which the species containing even numbers of metal atoms exhibit higher electron binding energies than the ones containing odd numbers of metal atoms. This result can be explained by the electron pairing effect, just like the pure Bi clusters, in which the EA of the odd numbered pure metal cluster is larger than that of the even one.[48,49] The reason is that the electron in doubly occupied highest-occupied molecular orbital (HOMO) will feel a stronger effective core potential due to less electron screening for electron in the same orbital than the open shell electrons. So it needs more energy to detach an electron from an anion with closed shell.

Another point is that the electron detachment threshold of every $Pb_mC_6F_5^-$ ($m = 1-4$) is comparatively higher than that of the corresponding naked lead clusters Pb_m^-.[31,33] The same result is obtained for Bi. This fact can be understood by the molecular orbital theory. After the bonding of Pb_m^- with the C_6F_5 group, the symmetries of the products are lowered, and

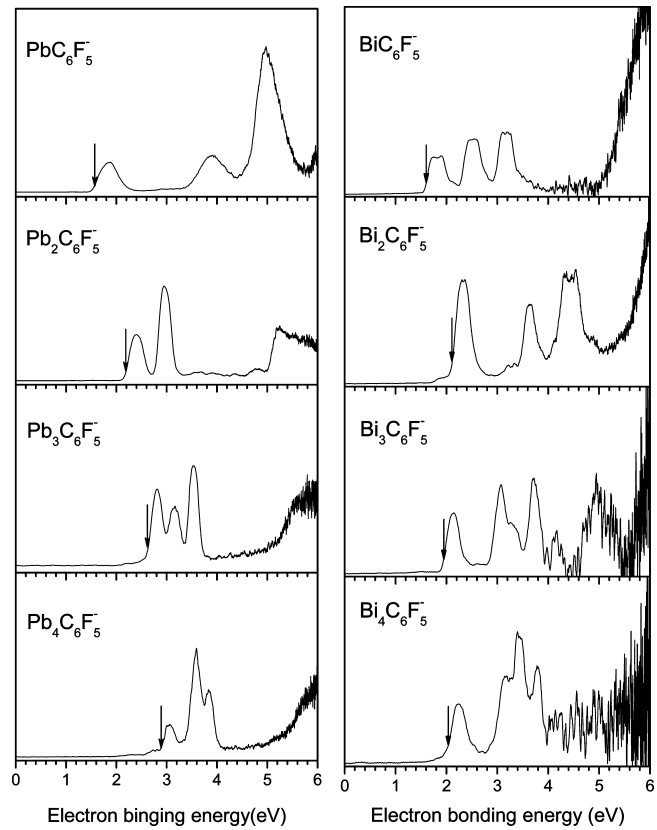

Figure 3. Photoelectron spectra of $Pb_mC_6F_5^-$ and $Bi_mC_6F_5^-$ ($m = 1-4$) at 193 nm (6.42 eV) photons.

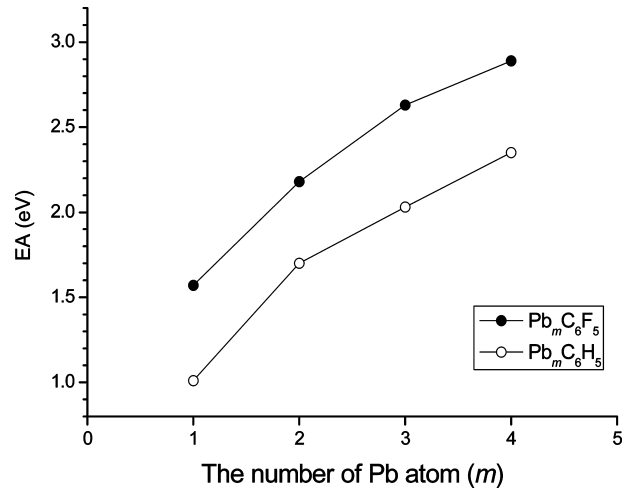

Figure 4. The comparison between the EAs of the $Pb_mC_6F_5$ and $Pb_mC_6H_5$ complexes.

the original degenerate orbitals (for example, $6p_x6p_y6p_z$ for Pb^-, $6p\pi$ for Pb_2^-, etc.) are transformed into nondegenerate ones. The MOs near the HOMO are rearranged and have a lower energy level due to the contribution of the formed Pb−C bond,[24,39] making the electron detachment threshold greater.

For $Pb_mC_6F_5$ ($m = 1-4$) complexes, the PE spectrum features (including the slow rising tails of the spectrum and the first and second spectrum peaks) are similar to those of $Pb_mC_6H_5^-$ ($m = 1-4$),[24] but the EAs of the formers are higher than those of the latters, respectively, as shown in Figure 4. This implies that the fluorine substitution strengthens metal binding with fluorinated benzene ring. The F atoms with higher electronegativity withdraw electron density from the aromatic system, and the carbon ring in the perfluorophenyl group becomes

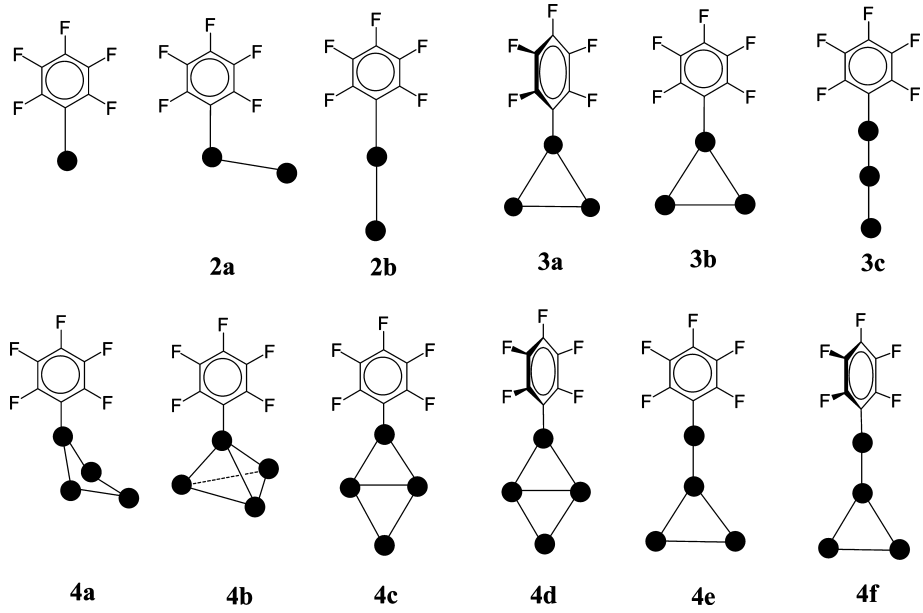

Figure 5. Optimized structures for neutral and anionic complexes of $Pb_mC_6F_5$ ($m = 1-4$). See Table 2 for structural parameters.

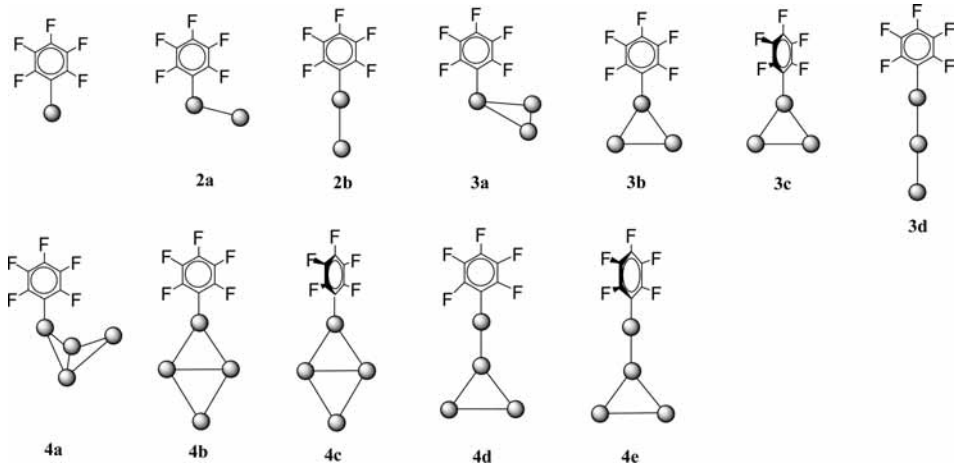

Figure 6. Optimized structures for neutral and anionic complexes of $Bi_mC_6F_5$ ($m = 1-4$). See Table 3 for structural parameters.

electron deficient. This result could lead to "spill-out" of electron density from the metal cluster into the carbon ring, to increase the electron binding energy. Therefore, the fluorinated phenyl has more effect on the lead clusters than the phenyl. In addition, it was reported that the phenyl group provided a single electron to combine with Pb_m through Pb−C σ bond.[24] We suppose that the C_6F_5 could adsorb on the surface of the lead cluster through a single Pb−C σ bond to form $Pb_mC_6F_5^-$ complexes. This idea will be further explained by the following theoretical investigation.

For $Bi_mC_6F_5^-$ complexes, it is also found that the electron detachment threshold of every $Bi_mC_6F_5^-$ ($m = 1-4$) is comparatively higher than that of the corresponding naked bismuth clusters Bi_m^-.[48,49] As shown in Figures 2 and 3, the PE spectrum features of $Bi_mC_6F_5^-$ (including the slow rising tails of the spectrum and the first and second spectrum peaks) show some similarities to those of Bi_{m+1}^-. This similarity can be explained as follows. The C_6F_5 group can be thought to act as an additional metal atom in $Bi_mC_6F_5^-$ complexes, and it contributes a single electron to bind with the metal cluster, like Bi atom binding with Bi_m^-. PES can probe the electronic structure of matter. The transition due to photodetachment occurs from the ground state of an anion to the ground and various excited states of the corresponding neutral. A PE spectrum is usually interpreted based on the single electron approximation, where single electron is detached from the occupied MO and the PE spectrum corresponding to the single electron is presented. Although this approximation is quite crude and ignores many factors, such as relaxation effects, multiplet splittings, and electron correlations, it still provides a useful mean to interpret the PE spectral features and to give the insight into the molecular bonding and electronic structure. Therefore, the similarity of the PE spectra between $Bi_mC_6F_5^-$ and Bi_{m+1}^- shows that the PE spectra of $Bi_mC_6F_5^-$ come from the MOs of the Bi cluster part in $Bi_mC_6F_5^-$. This idea will also be presented further by the following theoretical investigation.

4.3. Low-Energy Structures. To interpret the experimental results, the structures of the neutral and anion of $Pb_mC_6F_5$ and $Bi_mC_6F_5$ complexes ($m = 1-4$) are optimized by the DFT method. A variety of structures for both neutral and anion of the above complexes were considered. The optimized low-energy structures were shown in Figures 5 and 6, and their structural and energetic characteristics are summarized in Tables 2 and 3.

For all of the neutral $Pb_mC_6F_5$ complexes, the doublet-state configurations have lower energies than those of the quartet-state ones. For the anionic $Pb_mC_6F_5^-$ complexes, except $PbC_6F_5^-$, the singlet-state configurations have lower energies than the triplet-state ones. For $PbC_6F_5^-$, the triplet-state con-

TABLE 2: Various Structural and Energetic Characteristics for Neutral and Anionic Complexes of $Pb_mC_6F_5$ ($m = 1-4$)

	isomer	state	point group	R_{C-Pb} (Å)	ΔE^a (eV)	EA (eV) cal	EA (eV) exp[b]
PbC_6F_5		$^2B_1$	C_{2v}	2.32	0.00		1.60
$PbC_6F_5^-$		$^3B_2$	C_{2v}	2.42	0.00	1.80	
		$^1A_1$	C_s	2.41	0.60	1.20	
$Pb_2C_6F_5$	**2a**	$^2A''$	C_s	2.39	0.00	2.18	2.18
	2b	$^2B_1$	C_{2v}	2.28	0.86	2.40	
$Pb_2C_6F_5^-$	**2a**	$^1A'$	C_{2v}	2.44	0.00		
	2b	$^1A_1$	C_s	2.33	0.65		
$Pb_3C_6F_5$	**3a**	$^2B_1$	C_{2v}	2.26	0.01	2.68	2.63
	3b	$^2B_1$	C_{2v}	2.27	0.00	2.62	
	3c	$^2B_1$	C_{2v}	2.39	1.32	2.52	
$Pb_3C_6F_5^-$	**3a**	$^1A_1$	C_{2v}	2.33	0.00		
	3b	$^1A_1$	C_{2v}	2.35	0.05		
	3c	$^1A'$	C_{2v}	2.77	1.47		
$Pb_4C_6F_5$	**4a**	$^2A''$	C_s	2.32	0.00	2.90	2.89
	4b	$^2A''$	C_s	2.29	0.24	2.10	
	4c	$^2B_2$	C_{2v}	2.26	0.04	1.90	
	4d	$^2B_2$	C_{2v}	2.29	0.12	1.73	
	4e	$^2B_2$	C_{2v}	2.41	1.75	2.55	
	4f	$^2B_2$	C_{2v}	2.41	1.74	2.58	
$Pb_4C_6F_5^-$	**4a**	$^1A'$	C_s	2.37	0.00		
	4b	$^1A'$	C_s	2.36	1.04		
	4c	$^1A_1$	C_{2v}	2.26	2.11		
	4d	$^1A_1$	C_{2v}	2.33	2.07		
	4e	$^1A_1$	C_{2v}	2.56	1.04		
	4f	$^1A_1$	C_{2v}	2.57	1.29		

[a] ΔE is the difference of complex energy relative to the correspondingly lowest lying structure. [b] The uncertainty for the experimental EA is ±0.1 eV.

TABLE 3: Various Structural and Energetic Characteristics for Neutral and Anionic Complexes of $Bi_mC_6F_5$ ($m = 1-4$)

	isomer	state	point group	R_{C-Bi} (Å)	ΔE^a (eV)	EA (eV) cal	EA (eV) exp[b]
BiC_6F_5		$^3A_2$	C_{2v}	2.26	0.00	1.81	1.61
		$^1A_1$	C_{2v}	2.26	1.08	2.89	
$BiC_6F_5^-$		$^2B_2$	C_{2v}	2.29	0.00		
$Bi_2C_6F_5$	**2a**	$^2A''$	C_s	2.31	0.00	2.17	2.12
	2b	$^2A_2$	C_{2v}	2.47	0.91	2.71	
$Bi_2C_6F_5^-$	**2a**	$^1A'$	C_s	2.50	0.00		
	2b	$^1A_1$	C_{2v}	3.16	0.37		
$Bi_3C_6F_5$	**3a**	$^1A'$	C_s	2.32	0.00	2.06	1.96
	3b	$1A_1$	C_{2v}	2.49	1.85	2.92	
	3c	$1A_1$	C_{2v}	2.51	1.92	2.78	
	3d	$1A_1$	C_{2v}	2.31	2.20	2.66	
$Bi_3C_6F_5^-$	**3a**	$^2A''$	C_s	2.38	0.00		
	3b	$^2B_2$	C_{2v}	2.62	0.99		
	3c	$^2A_2$	C_{2v}	2.90	1.21		
	3d	$^2B_2$	C_{2v}	2.40	1.61		
$Bi_4C_6F_5$	**4a**	$^2A''$	C_s	2.32	0.00	2.11	2.05
	4b	$^2A''$	C_s	2.33	2.02	2.76	
	4c	$^2A''$	C_s	2.41	2.10	2.78	
	4d	$^2B_1$	C_{2v}	2.33	2.01	2.60	
	4e	$^2B_1$	C_{2v}	2.33	2.01	2.64	
$Bi_4C_6F_5^-$	**4a**	$^1A'$	C_s	2.35	0.00		
	4b	$^3B_2$	C_{2v}	2.58	1.37		
	4c	$^3B_2$	C_{2v}	2.67	1.42		
	4d	$^3B_2$	C_{2v}	2.47	1.52		
	4e	$^3B_2$	C_{2v}	2.50	1.48		

[a] ΔE is the difference of complex energy relative to the correspondingly lowest-lying structure. [b] The uncertainty for the experimental EA is ± 0.1 eV.

figuration has lower energy than the singlet-state one (see Table 2). This exception is due to the smaller size in $PbC_6F_5^-$, leading to an increase of electron−electron repulsion for the singlet state, and the triplet state is much more favorable. But this effect becomes relaxed if the HOMO of the complex becomes spatially large enough. For both neutral $Pb_mC_6F_5$ and anion $Pb_mC_6F_5^-$, their optimized structures are formed by C_6F_5 group coupling with the lead cluster through the Pb−C bond. The lowest energy structures are similar to the ones of $Pb_mC_6H_5$ complexes,[24] except the $Pb_2C_6F_5$ complex. For neutral $Pb_2C_6F_5$ and anion $Pb_2C_6F_5^-$, the lowest energy structure is isomer **2a** with C_s symmetry, in which the angle of C−Pb−Pb is 87°. Isomer **2b**, in which C−Pb−Pb is linear, is similar to the most likely structure of the $Pb_2C_6H_5$ complex which has C_{2v} symmetry, but it has higher energy than isomer **2a**.

For both neutral $Bi_mC_6F_5$ and anion $Bi_mC_6F_5^-$, their optimized structures have some similarities with the structures of neutral and anionic complexes of $Pb_mC_6F_5$, in which the C_6F_5 group couples with the bismuth atom through the Bi−C bond. For the neutral BiC_6F_5, the triplet-state configuration has lower energy than the singlet-state one (see Table 3), like $PbC_6F_5^-$ discussed above. This is because the neutral BiC_6F_5 and anion $PbC_6F_5^-$ are isoelectronic species. For neutral $Bi_2C_6F_5$ and anion $Bi_2C_6F_5^-$, isomer **2a** with C_s symmetry has the lowest energy, in which the angle of C−Bi−Bi is 110°. For neutral $Bi_3C_6F_5$ and the anion $Bi_3C_6F_5^-$, isomer **3a** with C_s symmetry is the lowest energy structure, in which the C_6F_5 group couples with the bismuth atom through the Bi−C bond and the plane of the C_6F_5 group is perpendicular to the face of Bi_3 group.

4.4. Assignments of the Complex Structures. In the following, we will confirm the structures of $M_mC_6F_5^-$ (M=Pb and Bi; $m = 1-4$) with the help of relativistic DFT. The assignment of the most likely structures of $M_mC_6F_5^-$ (M = Pb and Bi) is given on the basis of relative energies and comparisons of the theoretically calculated density-of-states (DOS) spectrum with the experimental PE spectra. This method of structural assignment has been widely used in cluster studies.[24,57,59−61] The EA is calculated as the difference between the total energies of the neutral and anion at their respective optimized structures. The theoretical DOS spectrum is shifted by setting the HOMO level of the spectrum to the negative of the VDE value for the complex. This is called theoretically generalized Koopmans theorem (GKT)[62]-shifted DOS.[63] Here it should be noticed that in comparison of the DOS spectrum with the PE spectrum, the important feature is the position of the electron binding energy corresponding to each spectrum and not the relative intensity of the spectrum.[63] The relative intensity also depends on other factors, such as the unknown orbital-dependent photodetachment cross-section. So here the DOS spectrum is plotted as the stick spectrum by aligning the HOMO level of anions with the threshold peak instead of the fitted DOS spectrum.[24] The stick spectrum is named the simulated spectrum based on Koopmans' theorem in the section. The comparisons of the simulated spectra based on Koopmans' theorem with experimental PE spectra of $M_mC_6F_5^-$ (M=Pb and Bi; $m = 1-4$) are shown in Figures 7−14.

$PbC_6F_5^-$. The calculations reveal that the structure of $PbC_6F_5^-$ with triplet state is in the ground state and has lower energy than the singlet state. For both neutral and anionic complexes, the lead atom couples with the C_6F_5 group in a planar through the Pb−C bond. The electron detachment thresholds of $PbC_6F_5^-$ with singlet and triplet state are 1.20 and 1.80 eV, respectively (see Table 2). The experimental result is 1.60 eV. Clearly, the electron detachment threshold of $PbC_6F_5^-$ with triplet state corresponds better to the experimental result than the one with singlet state. Figure 7 shows the comparison of the PE spectrum of $PbC_6F_5^-$ with the simulated spectrum based on Koopmans' theorem of $PbC_6F_5^-$ with triplet state. The distribution of the

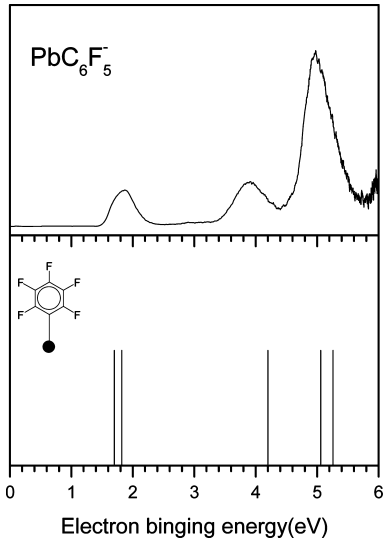

Figure 7. The comparison of PE spectrum of $PbC_6F_5^-$ with the simulated spectrum based on Koopmans' theorem for the structure of $PbC_6F_5^-$ with triplet state.

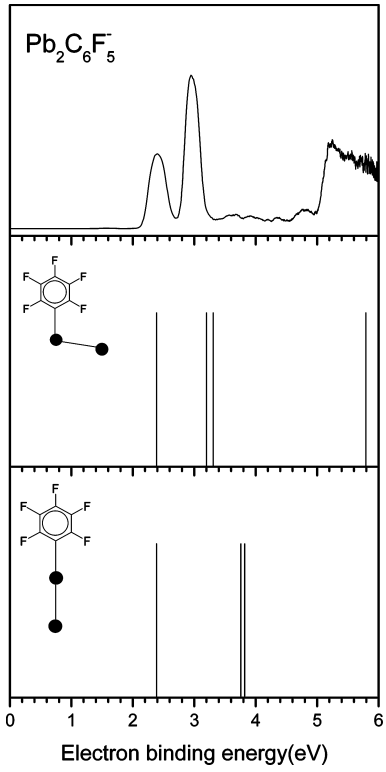

Figure 8. The comparison of PE spectrum of $Pb_2C_6F_5^-$ with the simulated spectra based on Koopmans' theorem for isomers **2a** and **2b** of $Pb_2C_6F_5^-$.

simulated spectrum agrees well with that of the experimental PE spectrum. It is suggested that only the anion $PbC_6F_5^-$ with triplet state contributes to the measured PE spectrum.

$Pb_2C_6F_5^-$. The planar structure (isomer **2a**) with C_s symmetry, in which the C_6F_5 group couples on the lead atom through the Pb−C bond, is clearly in the ground state for both neutral and anionic complexes of $Pb_2C_6F_5$. The energy differences between isomers **2a** and **2b** of both neutral and anionic complexes, and the calculated EAs are listed in Table 2. The calculated EAs of isomer **2a** and **2b** by the relativistic DFT are 2.18 and 2.40 eV, respectively. The experimental value is 2.18 eV. So the EA of isomer **2a** is in good agreement with the experimental result.

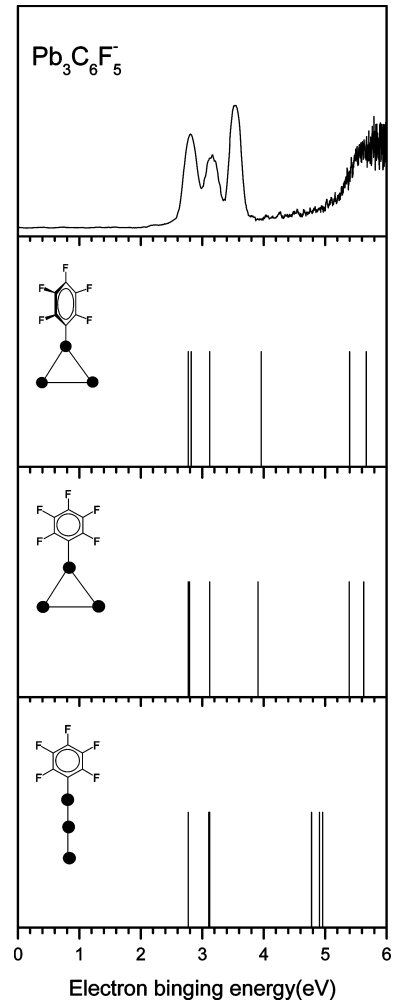

Figure 9. The comparison of PE spectrum of $Pb_3C_6F_5^-$ with the simulated spectra based on Koopmans' theorem for isomers **3a**−**3c** of $Pb_3C_6F_5^-$.

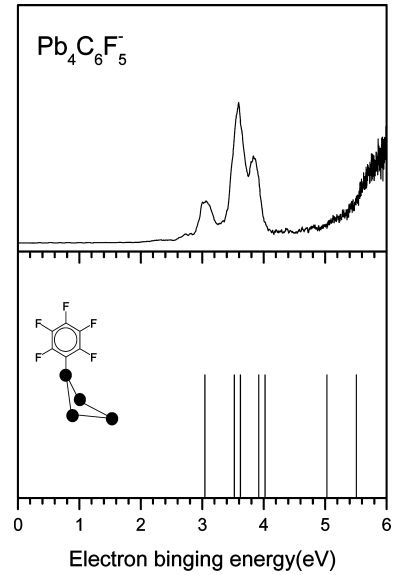

Figure 10. The comparison of PE spectrum of $Pb_4C_6F_5^-$ with the simulated spectrum based on Koopmans' theorem for the isomer **4a** of $Pb_4C_6F_5^-$.

The comparison of the PE spectrum with the theoretically simulated spectrum based on Koopmans' theorem for the isomer **2a** and **2b** of $Pb_2C_6F_5^-$ is presented in Figure 8. The distribution

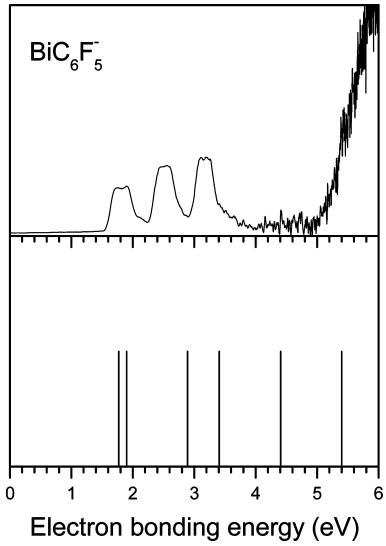

Figure 11. The comparison of PE spectrum of $BiC_6F_5^-$ with the simulated spectrum based on Koopmans' theorem for the optimized ground state structure of $BiC_6F_5^-$.

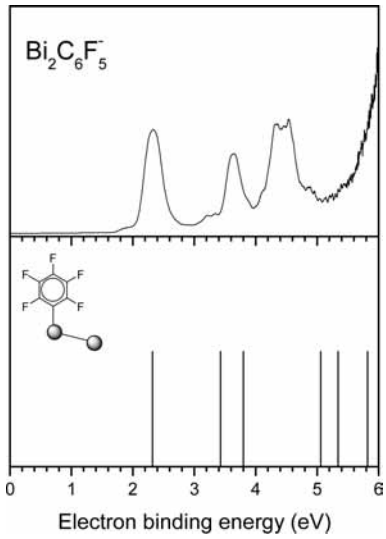

Figure 12. The comparison of PE spectrum of $Bi_2C_6F_5^-$ with the simulated spectrum based on Koopmans' theorem for isomer **2a** of $Bi_2C_6F_5^-$.

of the simulated spectrum of isomer **2a** agrees well with that of the experimental PE spectrum, while the one of isomer **2b** does not match the experimental PE spectrum. It is suggested that only isomer **2a** contributes to the measured PE spectrum.

$Pb_3C_6F_5^-$. The calculations reveal that the isomer **3a** has almost equal energy with isomer **3b** (the difference is 0.05 eV), and they are the two lowest energy structures. The calculated EAs of **3a** and **3b** are 2.68 and 2.62 eV respectively, which are both in good agreement with the experimental results of 2.63 eV. The EA of isomer **3c** is 2.52 eV, lower than the experimental value but close to the experimental value. The three simulated spectra based on Koopmans' theorem for isomers **3a**, **3b**, and **3c** are compared with experimental PE spectrum as shown in Figure 9. It can be concluded that the distributions of the simulated spectra for isomer **3a** and **3b** match the experimental result well, while the one of the simulated spectrum for isomer **3c** is not in agreement with the experimental PE spectrum. So it is suggested that both of the isomers **3a** and **3b** are presented in the product $Pb_3C_6F_5^-$.

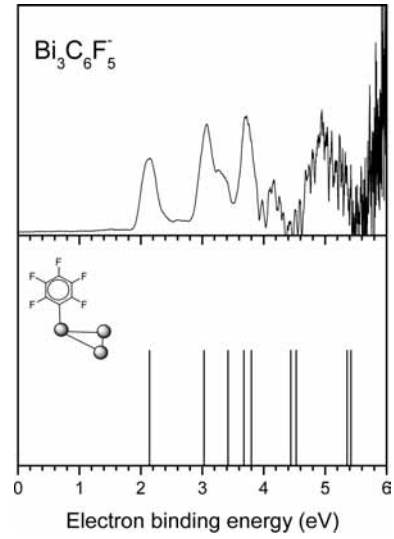

Figure 13. The comparison of PE spectrum of $Bi_3C_6F_5^-$ with the simulated spectrum based on Koopmans' theorem for isomer **3a** of $Bi_3C_6F_5^-$.

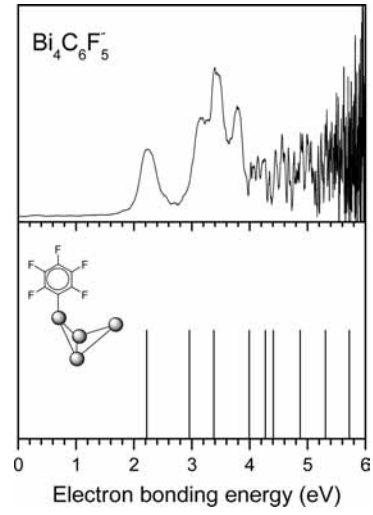

Figure 14. The comparison of PE spectrum of $Bi_4C_6F_5^-$ with the simulated spectrum based on Koopmans' theorem for isomer **4a** of $Bi_4C_6F_5^-$.

$Pb_4C_6F_5^-$. The calculations reveal that the structure of $Pb_4C_6F_5^-$ with ground state is isomer **4a.** As listed in Table 2, the EAs of isomers **4a**−**4f** are 2.90, 2.10, 1.90, 1.73, 2.55, and 2.58 eV, respectively. The experimental value is 2.89 eV. Obviously, the isomer **4a** corresponds better to the experimental result than the others. The simulated spectrum based on Koopmans' theorem of isomer **4a** is compared with experimental PE spectrum as shown in Figure 10. It is indicated that the simulated spectrum of isomer **4a** is in good agreement with measured PE spectrum. Thus, it is suggested that only isomer **4a** of anion $Pb_4C_6F_5^-$ contributes to the measured PE spectrum.

$BiC_6F_5^-$. The calculations indicate that for neutral BiC_6F_5, the structure with triplet state is in the ground state and has lower energy than the one with singlet state. For both neutral BiC_6F_5 and anion $BiC_6F_5^-$, the bismuth atom couples on the C_6F_5 group in a planar geometry through the Bi−C bond. The energy difference between the anion $BiC_6F_5^-$ and neutral BiC_6F_5 with triplet state is 1.81 eV and with the singlet state is 2.89 eV (see Table 3). The experimental value is 1.61 eV. So it can be concluded that the anion $BiC_6F_5^-$ becomes the neutral BiC_6F_5 with triplet state by photodetached an electron. The comparison

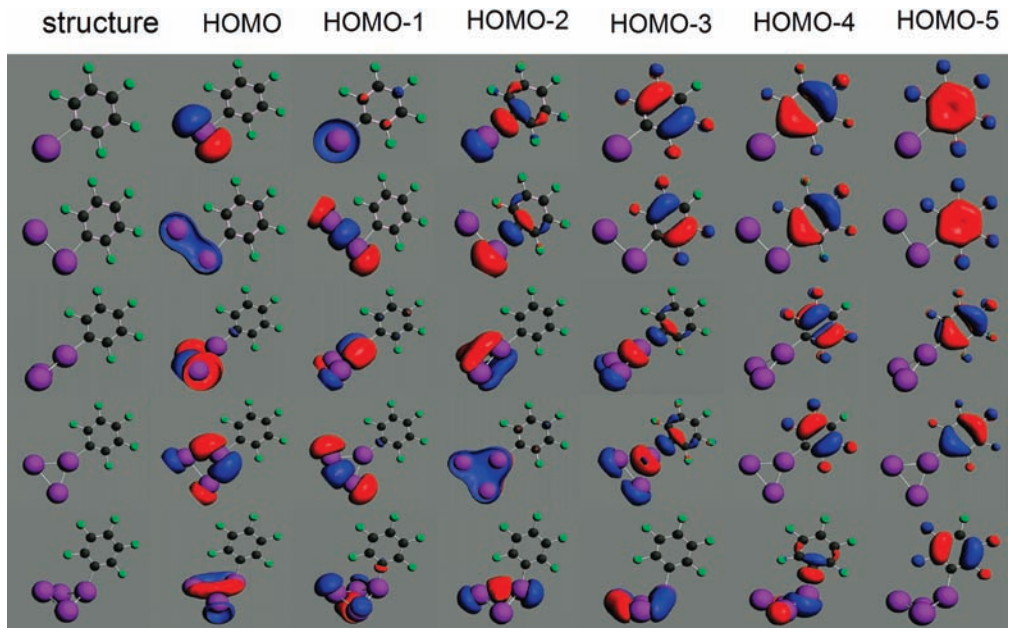

Figure 15. Molecular orbital pictures for the most likely structures of $Pb_mC_6F_5^-$ ($m = 1-4$) complexes.

between the PE spectrum of $BiC_6F_5^-$ and the simulated spectrum based on Koopmans' theorem for $BiC_6F_5^-$ is presented in Figure 11. It can be seen that the simulated spectrum agrees reasonably well with the experimental PE spectrum. Thus, it is suggested that only the anion $BiC_6F_5^-$ contributes to the measured PE spectrum.

$Bi_2C_6F_5^-$. The planar structure of isomer **2a** with C_s symmetry, in which the C_6F_5 group couples on the Bi atom through the Bi−C bond, is in the ground state for both neutral and anionic complexes. The energy differences between the anionic and neutral structures (corresponding to the calculated EAs) of isomer **2a** and **2b** are 2.17 and 2.71 eV, respectively (listed in Table 3). The experimental result is 2.12 eV. So the EA of isomer **2a** is in better agreement with the experimental result than that of isomer **2b**. The comparison between the PE spectrum of $Bi_2C_6F_5^-$ and the simulated spectrum based on Koopmans' theorem for the isomer **2a** is presented in Figure 12, and the energy gaps between the HOMO levels in the simulated spectrum of isomer **2a** agree well with the experimental PE spectrum. Thus, it is suggested that only the isomer **2a** contributes to the measured PE spectrum.

$Bi_3C_6F_5^-$. The calculations indicate that the isomer **3a** is the lowest energy structure for both neutral and anion of $Bi_3C_6F_5$ complex, and the energies of isomers **3b**−**3d** are much higher than that of isomer **3a** for both neutral and anion. The calculated EAs of isomers **3a**−**3d** are 2.06, 2.92, 2.78, and 2.66 eV, respectively, and the experimental result is 1.96 eV. Obviously, the EA of isomer **3a** is in agreement with the experimental result, and the EAs of the other isomers are much higher than the experimental value. The simulated spectrum based on Koopmans' theorem of isomer **3a** is compared with experimental PE spectrum as shown in Figure 13. The distribution of the simulated spectrum agrees reasonably well with that of the experimental PE spectrum. So it is suggested that the isomer **3a** is presented in the product $Bi_3C_6F_5^-$.

$Bi_4C_6F_5^-$. The calculations reveal that the lowest energy structure of neutral $Bi_4C_6F_5$ and anion $Bi_4C_6F_5^-$ is isomer **4a**. The other isomers of both neutrals and anions are much higher in energy than isomer **4a**. As listed in Table 3, the EAs of isomers **4a**−**4e** are 2.11, 2.78, 2.76, 2.60, and 2.64 eV, respectively. The experimental value is 2.05 eV. Obviously, the EA of isomer **4a** is much closer to the experimental value than the others. The simulated spectrum based on Koopmans' theorem of isomer **4a** is compared with experimental PE spectrum as shown in Figure 14. It is indicated that the simulated spectrum of isomer **4a** is in good agreement with measured PE spectrum. So it is suggested that the isomer **4a** is presented in the product $Bi_4C_6F_5^-$.

4.5. Orbital Composition and Bonding. We also analyzed the orbital compositions of the anionic complexes, and the calculated molecular orbital (MO) pictures for $M_mC_6F_5^-$ (M= Pb and Bi; $m = 1-4$) are given in Figures 15 and 16.

For $PbC_6F_5^-$ with the ground-state as shown in Figure 15, the HOMO and HOMO-1 are mostly from the $6p_x$ and $6p_y$ of the Pb atom, and they are nonbonding MOs for the Pb−C part. The HOMO-2 is formed by interaction of 6s and $6p_z$ of the Pb atom with $19A_1$ of C_6F_5, which is a σ MO for the Pb−C part. Following the HOMO-2, the inner MOs of $PbC_6F_5^-$ are only from the C_6F_5 part, which are nonbonding MOs for the Pb−C part. Therefore, the Pb atom and the C_6F_5 group bind together by the σ bond, in which the sp-hybridized orbital of the Pb atom interacts with the $19A_1$ of C_6F_5 (mainly formed with $2p_z$ orbital of the nearest C atom). As for $Pb_2C_6F_5^-$, the HOMO is from the $6p_x$ interaction of two Pb atoms, and the HOMO-1 is from the $6p_y$ interaction of two Pb atoms. These two MOs are local π-type and σ-type bonds between two Pb atoms, respectively. The HOMO-2 is formed by interaction of 6s and $6p_z$ of Pb atoms with $19A_1$ of C_6F_5, which is a σ MO for the Pb−C part. And the inner MOs are the nonbonding MOs for the Pb−C part, similar to the case of $PbC_6F_5^-$. Therefore, the Pb atom binds with the closest C atom of C_6F_5 by the σ bond, in which 6s and $6p_z$ orbitals of the Pb atom hybridize, and then binds with the $2p_z$ orbital of the closest C atom.

For $Pb_3C_6F_5^-$, there are two likely isomeric structures (**3a** and **3b**). So we investigated the MOs and bonding for these two isomers. The calculations show that the MOs near HOMO for isomer **3a** and **3b** are similar, as shown in Figure 15. So the analysis of the MO composition is only given for isomer **3a**. The HOMO, HOMO-1, and HOMO-2 are mostly the local MOs between Pb atoms. Only the HOMO-3 is a σ MO for the Pb−C part, and the inner MOs are also nonbonding MOs for the Pb−C part. So we conclude that in the $Pb_3C_6F_5^-$ complex the Pb_3

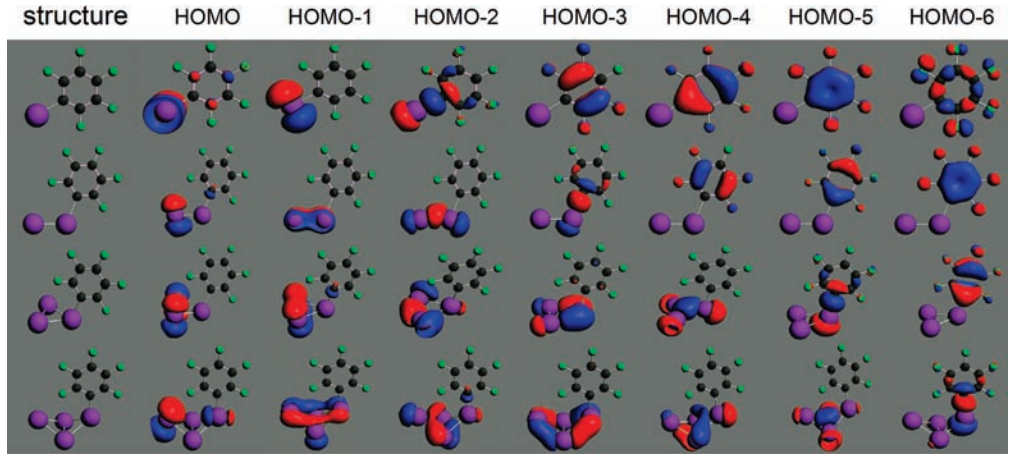

Figure 16. Molecular orbital pictures for the most likely structures of $Bi_mC_6F_5^-$ ($m = 1-4$) complexes.

cluster as a unit connects with the C_6F_5 group by the Pb−C σ bond. Similar cases can be seen for the $Pb_4C_6F_5^-$ complex, and there is only one σ MO for the Pb−C part. In general, it is presented that the number of outer local MOs of the $Pb_mC_6F_5^-$ complexes located in Pb atoms is equal to the number of Pb atoms. And there exists only one σ MO for the Pb−C part, which can be taken as evidence that C_6F_5 binds with lead clusters through the Pb−C σ bond. This Pb−C σ-bond interaction also influences the energy level of the outer MOs to result in the electron detachment thresholds of $Pb_mC_6F_5^-$ complexes being higher than those of Pb_m^-. Moreover, it is obvious that the lone-pair electron of fluorine atom in C_6F_5 does not influence the outer local MOs. This also provides evidence that the PE spectra of $Pb_mC_6F_5^-$ are similar to those of $Pb_mC_6H_5^-$ complexes.[24]

By the same analysis, it is found that the MOs of the $Bi_mC_6F_5^-$ complexes are similar to the ones of $Pb_mC_6F_5^-$ complexes as shown in Figure 16. The outer MOs of $Bi_mC_6F_5^-$ complexes all come from the Bi_m clusters, which are the local π-type and σ-type MOs between the Bi atoms. The inner MOs of $Bi_mC_6F_5^-$ complexes are only from the C_6F_5 part, which are nonbonding MOs for the Bi−C part. For each of the $Bi_mC_6F_5^-$ complexes, there exists only one σ MO for the Bi−C part, which can be taken as evidence that C_6F_5 binds with Bi clusters through the Bi−C σ bond. So the C_6F_5 group acts as an additional metal atom in these complexes to contribute a single electron binding with the metal fragment, and the PE spectra of $Bi_mC_6F_5^-$ and Bi_{m+1}^- present some similarities. However, the difference between $Pb_mC_6F_5^-$ and $Bi_mC_6F_5^-$ complexes is the number of the outer local MOs. For the $Bi_mC_6F_5^-$ complexes, the number of outer local MOs between Bi atoms is more than that between Pb atoms in $Pb_mC_6F_5^-$ complexes, for the Bi atom has one more p electron than Pb.

5. Conclusions

$Pb_mC_6F_5^-$ and $Bi_mC_6F_5^-$ ($m = 1-4$) complexes are produced by the reactions between hexafluorobenzene and metal (M = Pb and Bi) clusters generated by laser ablation of metal solid samples. The EAs of $Pb_mC_6F_5$ and $Bi_mC_6F_5$ ($m = 1-4$) are obtained from the experimental PE spectra using a 193 nm laser. It is found that the EAs of $Pb_mC_6F_5$ are much higher than that of pure Pb_m, and the PE spectra of $Bi_mC_6F_5^-$ are similar to those of Bi_{m+1}^- (including the slow rising tails of the spectrum and the first and second spectrum peaks).

By the combination of experimental and theoretical results, we elucidated the bindings, geometries, and electronic structures of $Pb_mC_6F_5^-$ and $Bi_mC_6F_5^-$ complexes. For the lowest energy structure of each species, the theoretical EA is in good agreement with the EA value obtained from the PE spectrum. By comparison of the experimentally measured PE spectrum with the simulated spectrum based on Koopmans' theorem calculated by the relativistic DFT, the most likely structures of $Pb_mC_6F_5$ and $Bi_mC_6F_5$ ($m = 1-4$) are assigned. Then, the MO analysis reveals the bonding mode of M-C bond in $M_mC_6F_5^-$ (M= Pb and Bi; $m = 1-4$) complexes. All of the results indicate that the C_6F_5 group acts as an additional metal atom in the $M_mC_6F_5^-$ complexes, and contributes a single electron to bind with the metal fragment through the M-C σ bond. This is in good agreement with the experimental results.

Acknowledgment. We gratefully acknowledge the support of the National Natural Science Foundation of China under Grant Nos. 20203020 and 20433080. We are grateful to Dr. Weijun Zheng for his advice on this paper.

References and Notes

(1) Xi, M.; Bent, B. E. *Surf. Sci.* **1992**, *278*, 19.
(2) Yang, M. X.; Xi, M.; Yuan, H. J.; Bent, B. E.; Stevens, P.; White, J. M. *Surf. Sci.* **1995**, *341*, 9.
(3) Syomin, D.; Kim, J.; Koel, B. E.; Ellison, G. B. *J. Phys. Chem. B* **2001**, *105*, 8387.
(4) Sauer, J. *Chem. Rev.* **1989**, *89*, 199.
(5) Szilagyi, R. K.; Frenking, G. *Organometallics* **1997**, *16*, 4807.
(6) Backvall, J. E.; Bokman, F.; Blomberg, M. R. A. *J. Am. Chem. Soc.* **1992**, *114*, 534.
(7) Dougherty, D. A. *Science* **1996**, *271*, 163.
(8) Loffreda, D. *Angew. Chem., Int. Ed.* **2006**, *45*, 6537.
(9) Kitagawa, S.; Kitaura, R.; Noro, S. *Angew. Chem., Int. Ed.* **2004**, *43*, 2334.
(10) Zhong, Q. L.; Zhang, B.; Ding, Y. M.; Liu, Y. L.; Rao, G. S.; Wang, G. F.; Ren, B.; Tian, Z. Q. *Acta Phys. Chim. Sin.* **2007**, *23*, 1432.
(11) Vattuone, L.; Gerbi, A.; Rocca, M.; Valbusa, U.; Pirani, F.; Vecchiocattivi, F.; Cappelletti, D. *Angew. Chem., Int. Ed.* **2004**, *43*, 5200.
(12) Hoshino, K.; Kurikawa, T.; Takeda, H.; Nakajima, A.; Kaya, K. *J. Phys. Chem.* **1995**, *99*, 3053.
(13) Kurikawa, T.; Hirano, M.; Takeda, H.; Yagi, K.; Hoshino, K.; Nakajima, A.; Kaya, K. *J. Phys. Chem.* **1995**, *99*, 16248.
(14) Kurikawa, T.; Takeda, H.; Hirano, M.; Judai, K.; Arita, T.; Nagao, S.; Nakajima, A.; Kaya, K. *Organometallics* **1999**, *18*, 1430.
(15) Gerhards, M.; Thomas, O. C.; Nilles, J. M.; Zheng, W. J.; Bowen, K. H. *J. Chem. Phys.* **2002**, *116*, 10247.
(16) Zheng, W. J.; Nilles, J. M.; Thomas, O. C.; Bowen, K. H. *J. Chem. Phys.* **2005**, *122*, 44306.
(17) Zheng, W. J.; Nilles, J. M.; Thomas, O. C.; Bowen, K. H. *Chem. Phys. Lett.* **2005**, *401*, 266.
(18) Pandey, R.; Rao, B. K.; Jena, P.; Blanco, M. A. *J. Am. Chem. Soc.* **2001**, *123*, 3799.
(19) Rao, B. K.; Jena, P. *J. Chem. Phys.* **2002**, *117*, 5234.
(20) Wu, D. Y.; Ren, B.; Jiang, Y. X.; Xu, X.; Tian, Z. Q. *J. Phys. Chem. A* **2002**, *106*, 9042.

(21) Kandalam, A. K.; Rao, B. K.; Jena, P.; Pandey, R. *J. Chem. Phys.* **2004**, *120*, 10414.
(22) Xing, X. P.; Liu, H. T.; Tang, Z. C. *Physchemcomm* **2003**, *6*, 32.
(23) Sun, S. T.; Xing, X. P.; Liu, H. T.; Tang, Z. C. *J. Phys. Chem. A* **2005**, *109*, 11742.
(24) Liu, H. T.; Xing, X. P.; Sun, S. T.; Gao, Z.; Tang, Z. C. *J. Phys. Chem. A* **2006**, *110*, 8688.
(25) Nakajima, A.; Taguwa, T.; Hoshino, K.; Sugioka, T.; Naganuma, T.; Oho, F.; Watanabe, K.; Nakao, K.; Konishi, Y.; Kishi, R.; Kaya, K. *Chem. Phys. Lett.* **1993**, *214*, 22.
(26) Ho, Y.-P.; Dunbar, R. C. *Int. J. Mass Spectrom.* **1999**, *182*−*183*, 175.
(27) Caraiman, D.; Koyanagi, G. K.; Bohme, D. K. *J. Phys. Chem. A* **2004**, *108*, 978.
(28) Dai, D. G.; Balasubramanian, K. *Chem. Phys. Lett.* **1997**, *271*, 118.
(29) Zhao, C. Y.; Balasubramanian, K. *J. Chem. Phys.* **2002**, *116*, 10287.
(30) Luder, C.; Meiwes-Broer, K. H. *Chem. Phys. Lett.* **1998**, *294*, 391.
(31) Gantefor, G.; Gausa, M.; Meiwes-Broer, K. H.; Lutz, H. O. *Z. Phys. D* **1989**, *12*, 405.
(32) Ho, J.; Polak, M. L.; Lineberger, W. C. *J. Chem. Phys.* **1992**, *96*, 144.
(33) Negishi, Y.; Kawamata, H.; Nakajima, A.; Kaya, K. *J. Electron Spectrosc. Relat. Phenom.* **2000**, *106*, 117.
(34) Venkatachalapathy, R.; Davila, G. P.; Prakash, J. *Electrochem. Commun.* **1999**, *1*, 614.
(35) Halligudi, S. B.; Kala Raj, N. K.; Rajani, R.; Unni, I. R.; Gopinathan, S. *Appl. Catal., A* **2000**, *204*, L1.
(36) Tang, I. N.; Castleman, A. W. *J. Chem. Phys.* **1972**, *57*, 3638.
(37) Guo, B. C.; Purnell, J. W.; Castleman, A. W. *Chem. Phys. Lett.* **1990**, *168*, 155.
(38) Xing, X.; Tian, Z.; Liu, H.; Tang, Z. *J. Phys. Chem. A* **2003**, *107*, 8484.
(39) Liu, X.-J.; Han, K.-L.; Sun, S.-T.; Tang, Z.-C.; Qin, Z.-B.; Cui, Z.-F. *J. Phys. Chem. A* **2008**, *112*, 6850.
(40) Liu, K.; Chien, C. L.; Searson, P. C.; Kui, Y.-Z. *Appl. Phys. Lett.* **1998**, *73*, 1436.
(41) Li, Y.; Wang, J.; Deng, Z.; Wu, Y.; Sun, X.; Yu, D.; Yang, P. *J. Am. Chem. Soc.* **2001**, *123*, 9904.
(42) Liu, X.-Y.; Zeng, J.-H.; Zhang, S.-Y.; Zheng, R.-B.; Liu, X.-M.; Qian, Y.-T. *Chem. Phys. Lett.* **2003**, *374*, 348.
(43) Tian, Y.; Meng, G.; Biswas, S. K.; Ajayan, P. M.; Sun, S.; Zhang, L. *Appl. Phys. Lett.* **2004**, *85*, 967.
(44) Patolsky, F.; Lieber, C. M. *Mater. Today* **2005**, *8*, 20.
(45) Geusic, M. E.; Freeman, R. R.; Duncan, M. A. *J. Chem. Phys.* **1988**, *88*, 163.
(46) Ross, M. M.; McElvany, S. W. *J. Chem. Phys.* **1988**, *89*, 4821.
(47) Rovner, L.; Drowart, A.; Drowart, J. *Trans. Faraday Soc.* **1967**, *63*, 2906.
(48) Polak, M., L.; Ho, J.; Gerber, G.; Lineberger, W. C. *J. Chem. Phys.* **1991**, *95*, 3053.
(49) Gausa, M.; Kaschner, R.; Seifert, G.; Faehrmann, J. H.; Lutz, H. O.; Meiwes-Broer, K. H. *J. Chem. Phys.* **1996**, *104*, 9719.
(50) Gao, L.; Li, P.; Lu, H.; Li, S. F.; Guo, Z. X. *J. Chem. Phys.* **2008**, *128*, 194304.
(51) Xing, X. P.; Tian, Z. X.; Liu, P.; Gao, Z.; Zhu, Q.; Tang, Z. C. *Chin. J. Chem. Phys* **2002**, *15*, 83.
(52) Xing, X. P.; Liu, H. T.; Sun, S. T.; Cao, Y. L.; Tang, Z. C. *Chin. J. Chem. Phys.* **2004**, *17*, 321.
(53) Perdew, J. P.; Wang, Y. *Phys. Rev. B* **1992**, *45*, 13244.
(54) van Lenthe, E.; Baerends, E. J.; Snijders, J. G. *J. Chem. Phys.* **1993**, *99*, 4597.
(55) Vrije Universiteit, ADF 2005, SCM, Theoretical Chemistry, Amsterdam, Netherland (www.scm.com).
(56) BelBruno, J. J. *Surf. Sci.* **2005**, *577*, 167.
(57) Li, J.; Li, X.; Zhai, H.-J.; Wang, L.-S. *Science* **2003**, *299*, 864.
(58) Liu, H. T.; Sun, S. T.; Xing, X. P.; Tang, Z. C. *Rapid Commun. Mass Spectrom.* **2006**, *20*, 1899.
(59) Li, X.; Kiran, B.; Li, J.; Zhai, H. J.; Wang, L. S. *Angew. Chem.* **2002**, *41*, 4786.
(60) Wang, L. S.; Wang, X. B.; Wu, H. B.; Cheng, H. S. *J. Am. Chem. Soc.* **1998**, *120*, 6556.
(61) Häkinen, H.; Moseler, M.; Landman, U. *Phys. Rev. Lett.* **2002**, *89*, 033401.
(62) Tozer, D. J.; Handy, N. C. *J. Chem. Phys.* **1998**, *108*, 2545.
(63) Hakkinen, H.; Yoon, B.; Landman, U.; Li, X.; Zhai, H. J.; Wang, L. S. *J. Phys. Chem. A* **2003**, *107*, 6168.

JP8099626